

Technical Notes

TECHNICAL NOTES are short manuscripts describing new developments or important results of a preliminary nature. These Notes cannot exceed six manuscript pages and three figures; a page of text may be substituted for a figure and vice versa. After informal review by the editors, they may be published within a few months of the date of receipt. Style requirements are the same as for regular contributions (see inside back cover).

Induced Velocity in the Plane of an Elliptically Loaded Lifting Line

T. Sugimoto*

Kanagawa University, Yokohama 221-8686, Japan

Introduction

PRANDTL'S lifting-line theory¹⁻³ is no doubt one of the most important contributions to fluid mechanics in the past century. Inspired by Lanchester's physical insight,⁴ Prandtl and his collaborators developed the theory to predict the lift and induced drag of a wing with a finite span. Although some of his assumptions were introduced without sufficient validation at the moment of birth, the theory was later mathematically justified such that it has a sound basis on physics (for example, see van Dyke⁵ and Saffman⁶). Even now Prandtl's lifting-line theory is evolving and survives through competition with modern numerical wing theories.⁷ The theory has been used not only to predict three-dimensional aerodynamic characteristics but also to solve inverse problems and so on. There are, however, not so many applications to study flowfield around wings of finite spans, although the lifting-line theory has its root in physical intuition on flowfield around a three-dimensional wing. We shall review very briefly the former efforts to derive analytical formulas to describe several aspects of the induced flowfield around an elliptically loaded lifting line, which is well known to minimize induced drag of a single wing. From the early stages of development of the theory, a couple of formulas are known. Glauert⁸ summarizes the formulas to describe the induced velocity field in the transverse plane on which a bound vortex is placed and that in the Trefftz plane as well as the induced velocity upon the x axis. As recently as 1985, Phillips⁹ put forward the closed-form formula for the downwash in the plane of symmetry of an elliptically loaded wing. The present Note adds another formula that depicts the distribution of induced velocity in the plane of an elliptically loaded lifting line and its wake with special reference to the singularities at the edges of the vortex sheet. The newly derived formula would serve as a basis of estimating interaction among wings and also a test bed for modern numerical wing theories.

Derivation of Formula

This study uses the coordinate system after the conventional aeronautics. A lifting line or a wing is placed upon a line segment $[-1, 1]$ of a y axis. As we shall derive velocity field in $z = 0$ plane, we denote induced velocity simply by $w(x, y)$.

Prandtl's lifting-line theory can be described within the framework of inviscid vortex dynamics.⁶ The following volume integral gives forces acting on a wing:

Received 17 October 2001; revision received 4 February 2002; accepted for publication 4 March 2002. Copyright © 2002 by the American Institute of Aeronautics and Astronautics, Inc. All rights reserved. Copies of this paper may be made for personal or internal use, on condition that the copier pay the \$10.00 per-copy fee to the Copyright Clearance Center, Inc., 222 Rosewood Drive, Danvers, MA 01923; include the code 0001-1452/02 \$10.00 in correspondence with the CCC.

*Professor, Faculty of Engineering; currently Visiting Scholar, Department of Applied Mathematics and Theoretical Physics, University of Cambridge, Cambridge, England CB3 9EW, United Kingdom; take@ie.kanagawa-u.ac.jp. Member AIAA.

$$\mathbf{F} = \rho \int \mathbf{u} \times \boldsymbol{\omega} dV \quad (1)$$

where \mathbf{F} , ρ , \mathbf{u} , and $\boldsymbol{\omega}$ denote an aerodynamic force vector, air density, a velocity vector, and a vorticity vector, respectively. The velocity vector and the vorticity vector are interrelated by

$$\boldsymbol{\omega} = \nabla \times \mathbf{u} \quad (2)$$

When vorticity distribution is known, Biot-Savart's relation, the inverted version of Eq. (2), gives the induced velocity \mathbf{u} :

$$\mathbf{u}(\mathbf{r}) = \frac{1}{4\pi} \int \frac{\boldsymbol{\omega}(\mathbf{r}') \times (\mathbf{r} - \mathbf{r}')}{|\mathbf{r} - \mathbf{r}'|^3} dV(\mathbf{r}') \quad (3)$$

where \mathbf{r} and \mathbf{r}' denote the position vectors of \mathbf{u} and $\boldsymbol{\omega}$, respectively.

In our problem the vortices bounded upon the wing is give by using the circulation $\gamma(y)$:

$$\boldsymbol{\omega} = [0, \gamma(y), 0] \quad \text{for } y \in [-1, 1] \quad (4)$$

where

$$\gamma(y) = (\epsilon u \gamma_0 / 2) \sqrt{1 - y^2} \quad (5)$$

parameters ϵ , u , and γ_0 designate the ratio of root chord to semispan, flight velocity, and the circulation at the wing root, respectively. The parameter ϵ is related to the aspect ratio \mathcal{AR} in case of an elliptic wing:

$$\epsilon = 4/\pi \mathcal{AR}$$

On the other hand, the wake consists of changes in the vorticity shed from the wing:

$$\begin{aligned} \boldsymbol{\omega} &= \left[-\frac{d\gamma(y)}{dy}, 0, 0 \right] \\ &= \left(-\frac{\epsilon u \gamma_0}{2} \frac{d}{dy} \{ \sqrt{1 - y^2} \}, 0, 0 \right) \\ &\quad \text{for } x \times y \in [0, \infty) \times [-1, 1] \quad (6) \end{aligned}$$

Let us start from substituting vorticity distribution equations (4) and (6) for Eq. (3), and the following integral calculates velocity induced at a field point (x, y) by these vortices:

$$\begin{aligned} w(x, y) &= \frac{\epsilon \gamma_0}{8\pi} \int_{-1}^1 \frac{-\epsilon x \sqrt{1 - \eta^2}}{[\epsilon^2 x^2 - (y - \eta)^2]^{\frac{3}{2}}} d\eta \\ &\quad - \frac{\epsilon \gamma_0}{8\pi} \int_{-1}^1 \int_0^\infty \frac{y - \eta}{[(\epsilon x - \xi)^2 - (y - \eta)^2]^{\frac{3}{2}}} \frac{d}{d\eta} \{ \sqrt{1 - \eta^2} \} d\xi d\eta \end{aligned}$$

Integrating the second term on the right-hand side of the preceding equation in terms of ξ with some algebra as well, one obtains the induced velocity in a more concise and nondimensional form g :

$$\begin{aligned} g(x, y) &= \frac{8\pi}{\epsilon \gamma_0} w(x, y) \\ &= \int_{-1}^1 \sqrt{1 - \eta^2} \left[1 + \frac{\epsilon x}{\sqrt{\epsilon^2 x^2 + (y - \eta)^2}} \right] \frac{d\eta}{(y - \eta)^2} \quad (7) \end{aligned}$$

where we take Hadamard's finite part of the preceding improper integral.

Because the whole situation is symmetric about $y = 0$ plane, the following derivation shall be confined in the case of nonnegative y for the brevity of description:

The first term on the right-hand side of Eq. (7) can be integrated in terms of elementary functions, e.g., by use of complex-integral technique:

$$\int_{-1}^1 \frac{\sqrt{1-\eta^2}}{(y-\eta)^2} d\eta = \begin{cases} -\pi + \pi y / \sqrt{y^2-1} & \text{for } y > 1 \\ -\pi & \text{for } y \in [-1, 1] \end{cases} \quad (8)$$

The second term on the right-hand side of Eq. (7) can be expressed by the complete elliptic integrals. First integration by part yields

$$\begin{aligned} & \int_{-1}^1 \frac{\epsilon x}{\sqrt{\epsilon^2 x^2 + (y-\eta)^2}} \frac{\sqrt{1-\eta^2}}{(y-\eta)^2} d\eta \\ &= \epsilon x y \int_{-1}^1 \frac{d\eta}{(y-\eta)\sqrt{(1-\eta^2)[\epsilon^2 x^2 + (y-\eta)^2]}} \\ & - \epsilon x \int_{-1}^1 \frac{d\eta}{\sqrt{(1-\eta^2)[\epsilon^2 x^2 + (y-\eta)^2]}} \\ & - \epsilon x \int_{-1}^1 \frac{\sqrt{1-\eta^2}}{[\epsilon^2 x^2 + (y-\eta)^2]^{\frac{3}{2}}} d\eta \end{aligned} \quad (9)$$

For $y \in [0, 1]$ one has to eliminate the singularity in the first integral on the right-hand side of Eq. (9). This will be done later.

Let us introduce the following change of variables:

$$\eta = (\sigma + \tau)/(1 + \sigma\tau)$$

where

$$\sigma = \delta - \sqrt{\delta^2 - 1}, \quad \delta = \frac{\epsilon^2 x^2 + y^2 + 1}{2y}$$

Changing variables from η to τ and noting the symmetry of the integrand in Eq. (9), one can rewrite Eq. (9) in the following:

$$\begin{aligned} & 2 \frac{\epsilon x y (y - \sigma)(1 - \sigma^2)}{1 - \sigma y} \int_0^1 \frac{1}{(y - \sigma)^2 - (1 - \sigma y)^2 \tau^2} \\ & \times \frac{d\tau}{\sqrt{(1 - \tau^2)(C_1 + C_2 \tau^2)}} \\ & - 2 \frac{\epsilon x \sqrt{1 - \sigma^2}}{1 - \sigma y} \int_0^1 \frac{d\tau}{\sqrt{(1 - \tau^2)(C_1 + C_2 \tau^2)}} \\ & - 2 \epsilon x (1 - \sigma^2)^{\frac{3}{2}} \int_0^1 \frac{\sqrt{1 - \tau^2}}{(C_1 + C_2 \tau^2)^{\frac{3}{2}}} d\tau \end{aligned} \quad (10)$$

where

$$C_1 = 2y(\delta - \sigma) - 1 + \sigma^2, \quad C_2 = 2y\sigma(\delta\sigma - 1) + 1 - \sigma^2$$

To obtain the standard forms of the complete elliptic integrals, we shall introduce another change of variables:

$$\tau^2 = 1 - u^2$$

Some algebra in Eq. (10) leads to the following:

$$\begin{aligned} & 2 \frac{\epsilon x y (y - \sigma)(1 - \sigma^2)^{\frac{3}{2}}}{(1 - \sigma y)(1 - \sigma^2)(y^2 - 1)\sqrt{C_1 + C_2}} \\ & \times \int_0^1 \frac{du}{(1 + Cu^2)\sqrt{(1 - u^2)(1 - k^2 u^2)}} \\ & - 2 \frac{\epsilon x}{1 - \sigma y} \sqrt{\frac{1 - \sigma^2}{C_1 + C_2}} \int_0^1 \frac{du}{\sqrt{(1 - u^2)(1 - k^2 u^2)}} \\ & - 2 \epsilon x \left(\frac{1 - \sigma^2}{C_1 + C_2} \right)^{\frac{3}{2}} \int_0^1 \frac{u^2 du}{\sqrt{(1 - u^2)(1 - k^2 u^2)^3}} \end{aligned} \quad (11)$$

where

$$\begin{aligned} C &= \frac{(1 - \sigma y)^2}{(1 - \sigma^2)(y^2 - 1)} \\ k^2 &= \frac{C_2}{C_1 + C_2} \\ &= \frac{\sigma(1 - \sigma y)}{(1 - \sigma^2)y} \end{aligned}$$

To arrive at the final form, we need to use standard formulas on the complete elliptic integrals such as

$$\begin{aligned} & \int_0^1 \frac{du}{(1 + Cu^2)\sqrt{(1 - u^2)(1 - k^2 u^2)}} = \frac{k^2}{k^2 + C} \mathbf{K}(k^2) \\ & + \left(\frac{1}{1 + C} - \frac{k^2}{k^2 + C} \right) \mathbf{\Pi}(n, k^2) \end{aligned}$$

$$\int_0^1 \frac{u^2 du}{\sqrt{(1 - u^2)(1 - k^2 u^2)^3}} = \frac{1}{(1 - k^2)k^2} \mathbf{E}(k^2) - \frac{1}{k^2} \mathbf{K}(k^2)$$

$$n = \frac{1 - \sigma y}{y(y - \sigma)}$$

Functions \mathbf{K} , \mathbf{E} , and $\mathbf{\Pi}$ are the complete elliptic integrals of the first, second, and third kind, respectively, that is,

$$\int_0^1 \frac{du}{\sqrt{(1 - u^2)(1 - k^2 u^2)}} = \mathbf{K}(k^2)$$

$$\int_0^1 \sqrt{\frac{1 - k^2 u^2}{1 - u^2}} du = \mathbf{E}(k^2)$$

$$\int_0^1 \frac{du}{(1 - nu^2)\sqrt{(1 - u^2)(1 - k^2 u^2)}} = \mathbf{\Pi}(n, k^2)$$

A few more manipulation leads us to the final form of the second term on the right-hand side of Eq. (7):

$$\begin{aligned} & \frac{2\epsilon x}{\{[\epsilon^2 x^2 + (y - 1)^2][\epsilon^2 x^2 + (y + 1)^2]\}^{\frac{1}{4}}} \left[\frac{y}{y - \sigma} \mathbf{\Pi}(n, k^2) \right. \\ & \left. + \frac{\sigma y}{1 - \sigma y} \mathbf{K}(k^2) - \frac{(1 - \sigma^2)y}{(1 - \sigma y)(y - \sigma)} \mathbf{E}(k^2) \right] \end{aligned} \quad (12)$$

By virtue of Eqs. (8) and (12), the nondimensional induced velocity is given by

$$\begin{aligned} g(x, y) &= -\pi + \pi \frac{y}{\sqrt{y^2 - 1}} \\ & + \frac{2\epsilon x}{\{[\epsilon^2 x^2 + (y - 1)^2][\epsilon^2 x^2 + (y + 1)^2]\}^{\frac{1}{4}}} \left[\frac{y}{y - \sigma} \mathbf{\Pi}(n, k^2) \right. \\ & \left. + \frac{\sigma y}{1 - \sigma y} \mathbf{K}(k^2) - \frac{(1 - \sigma^2)y}{(1 - \sigma y)(y - \sigma)} \mathbf{E}(k^2) \right] \end{aligned} \quad (13)$$

for $y > 1$.

In case $1 \geq y \geq 0$ we need to modify the complete elliptic integral of the third kind to eliminate the singularity:

$$\Pi(n, k^2) = \mathbf{K}(k^2) - \Pi(N, k^2)$$

where

$$\begin{aligned} N &= \frac{k^2}{n} \\ &= \frac{\sigma(y - \sigma)}{1 - \sigma^2} \end{aligned}$$

This identity is not valid if n approaches unity as will be shown later. Using the preceding relation and Eq. (8), one obtains the result for $1 \geq y \geq 0$:

$$\begin{aligned} g(x, y) &= -\pi + \frac{2\epsilon x}{\{[\epsilon^2 x^2 + (y - 1)^2][\epsilon^2 x^2 + (y + 1)^2]\}^{\frac{1}{4}}} \\ &\times \left[-\frac{y}{y - \sigma} \Pi(N, k^2) + \frac{(1 - \sigma^2)y}{(y - \sigma)(1 - \sigma y)} \mathbf{K}(k^2) \right. \\ &\left. - \frac{(1 - \sigma^2)y}{(1 - \sigma y)(y - \sigma)} \mathbf{E}(k^2) \right] \end{aligned} \quad (14)$$

To get the reduced form for $y = 0$, it is necessary to tend y to zero with special cares on the limiting procedure. This will be shown in the next section.

Limiting Cases

In this section we shall derive limiting values at edges of the vortex sheet and upon the x axis. The former reveals the singularity of flowfield, whereas the latter corresponds to the known form.⁸

If we let y tend to unity in Eq. (14), we obtain the limiting value approaching the edge of the vortex sheet from its interior:

$$g(x, 1) = -\pi + \frac{2\epsilon x}{[\epsilon^2 x^2 (\epsilon^2 x^2 + 4)]^{\frac{1}{4}}} \left\{ \frac{1 + \sigma}{1 - \sigma} [\mathbf{K}(k^2) - 2\mathbf{E}(k^2)] \right\} \quad (15)$$

because

$$\begin{aligned} \lim_{y \rightarrow 1} \Pi(N, k^2) &= \int_0^1 \frac{du}{\sqrt{(1 - u^2)(1 - k^2 u^2)^3}} \\ &= \frac{1}{1 - k^2} \mathbf{E}(k^2) \\ \lim_{y \rightarrow 1} k^2 &= \frac{\sigma}{1 + \sigma} \end{aligned}$$

On the other hand, the approach from the exterior of the vortex sheet exhibits such a singular behavior as follows:

$$\lim_{y \rightarrow 1} \Pi(n, k^2) = \mathbf{K}(k^2) - \frac{1}{1 - k^2} \mathbf{E}(k^2) + \frac{1}{\sqrt{1 - k^2}} \lim_{u \rightarrow 1} \frac{1}{\sqrt{1 - u^2}} \quad (16)$$

The third term on the right-hand side in Eq. (16) diverges, whereas the first two terms remain regular. This diverging character is a typical edge singularity as is seen in Eq. (8). As a matter of course, the interior value coincides with the exterior value except the singularity and the singularities upstream cancel out.

We shall derive the limiting form of Eq. (14) for $y = 0$:

$$\begin{aligned} g(x, 0) &= -\pi - \frac{2\epsilon x}{\sqrt{\epsilon^2 x^2 + 1}} \times \lim_{y \rightarrow 0} \frac{y}{y - \sigma} [\Pi(N, k^2) \\ &- \mathbf{K}(k^2) + \mathbf{E}(k^2)] \end{aligned}$$

because

$$\begin{aligned} \lim_{y \rightarrow 0} \sigma &= \lim_{y \rightarrow 0} \left\{ \delta - \delta \sqrt{1 - \delta^{-2}} \right\} \\ &= \lim_{\delta \rightarrow \infty} \left\{ \delta - \delta \sqrt{1 - \delta^{-2}} \right\} \\ &= 0 \end{aligned}$$

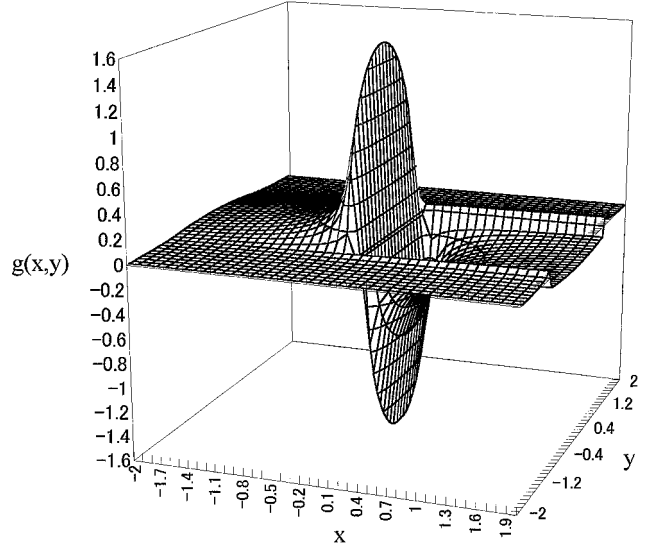


Fig. 1 Distribution of nondimensional induced velocity in the plane of an elliptically loaded lifting line and its wake.

On the other hand, the following also holds:

$$\begin{aligned} \lim_{y \rightarrow 0} \frac{\sigma}{y} &= \lim_{y \rightarrow 0} \frac{\delta - \delta \sqrt{1 - \delta^{-2}}}{y} \\ &= \lim_{y \rightarrow 0} \frac{\delta - \delta [1 - 1/2\delta^2 + \mathcal{O}(\delta^{-4})]}{y} \\ &= \lim_{y \rightarrow 0} \frac{1}{2y\delta} \\ &= \frac{1}{\epsilon^2 x^2 + 1} \end{aligned}$$

$$\begin{aligned} \lim_{y \rightarrow 0} \Pi(N, k^2) &= \Pi(0, k^2) \\ &= \mathbf{K}(k^2) \end{aligned}$$

where

$$\lim_{y \rightarrow 0} k^2 = \frac{1}{\epsilon^2 x^2 + 1}$$

Therefore, we obtain the limiting value on the x axis:

$$\begin{aligned} g(x, 0) &= -\pi - 2 \frac{\sqrt{\epsilon^2 x^2 + 1}}{\epsilon x} \mathbf{E}(k^2) \\ &= -\pi - 2 \operatorname{sgn}(x) \frac{\mathbf{E}(k^2)}{\sqrt{1 - k^2}} \end{aligned} \quad (17)$$

This corresponds to the classical result.⁸

Results

Figure 1 shows the distribution of induced velocity in the plane of an elliptically loaded lifting line and its wake by use of the newly derived formulas (13), (14), (15), (17), and their mirror images.

Conclusions

Modern computer environments offer easily accessible libraries to calculate the complete elliptic integrals. Researchers also have access to several symbolic manipulation systems that carry out calculation of the complete elliptic integrals immediately. Thus there is no difficulty in depicting the entire flowfield as in Fig. 1 very accurately. This flowfield itself might be much too simple, but it serves in several ways: it is useful to verify the accuracy of a numerical method; it is also useful to analytically understand the physical model, for example, the edge singularity as is referred to in the preceding section; it might well be useful at the conceptual design stage to consider the interaction of wings.

References

- ¹Prandtl, L., "Flüssigkeitsbewegung," *Handwörterbuch der Naturwissenschaften*, Vol. 4, Gustav Fischer, Jena, Germany, 1913, pp. 101–140.
- ²Betz, A., "Untersuchungen von Tragflächen mit Verwundenen und nach Rückwärts Gerichteten Enden," *Zeitschrift für Flugtechnik & Motorluftschiffahrt*, Vol. 5, 1914, pp. 16, 17.
- ³Prandtl, L., *Tragflächentheorie I. Mitteilung, Nachrichten der Gesellschaft der Wissenschaften zu Göttingen, Mathematisch-Physikalisch Klasse*, 1918, pp. 151–177.
- ⁴Lanchester, F. W., *Aerodynamics*, Constable and Co., London, 1907, pp. 139–178.
- ⁵van Dyke, M., *Perturbation Methods in Fluid Mechanics*, Parabolic Press, Stanford, CA, 1975, pp. 167–176.
- ⁶Saffman, P. G., *Vortex Dynamics*, Cambridge Univ. Press, Cambridge, England, U.K., 1992, pp. 95–115.
- ⁷Phillips, W. F., and Snyder, D. O., "Modern Adaptation of Prandtl's Classic Lifting-Line Theory," *Journal of Aircraft*, Vol. 37, No. 4, 2000, pp. 662–670.
- ⁸Glauert, H., *The Elements of Aerofoil and Airscrew Theory*, Cambridge Univ. Press, Cambridge, England, U.K., 1948, pp. 125–170.
- ⁹Phillips, J. D., "Downwash in the Plane of Symmetry of an Elliptically Loaded Wing," NASA-TP-2414, Jan. 1985.

A. Plotkin
Associate Editor

Assessment of Reaction Mechanisms for Counterflow Methane–Air Partially Premixed Flames

H. S. Xue* and S. K. Aggarwal†
University of Illinois at Chicago,
Chicago, Illinois 60607

R. J. Osborne‡ and T. M. Brown‡
NASA Marshall Space Flight Center,
Huntsville, Alabama 35812

and
R. W. Pitz§

Vanderbilt University, Nashville, Tennessee 37325

Introduction

PARTIALLY premixed flames (PPF) are hybrid flames containing multiple reaction zones. These flames are of fundamental importance to the phenomena of nonpremixed flame stabilization and liftoff, spray combustion, and localized extinction and reignition in turbulent flames. A double flame containing a fuel-rich premixed reaction zone that synergistically interacts with a nonpremixed reaction zone is an example of a partially premixed flame. Because these flames are characterized by thermochemical interactions between the reaction zones that involve the transport of both stable and radical species, it is essential that the simulation of their structure employ a reliable and detailed chemistry model. Our previous investigation¹ of PPFs in a counterflow configuration focused on the capability of five different reaction mechanisms for predicting the detailed structure of methane–air PPF for

a range of strain rates and equivalence ratios. The reaction mechanisms included the C_1 and C_2 mechanisms of Peters, which were used in our previous investigation,¹ GRI-2.11 and GRI-3.0 mechanisms (data available online at <http://www.me.berkeley.edu/gri-mech/> [cited 1 June 2001]), and a 12-step reduced mechanism.² The C_1 mechanism involves only C_1 species and 52 elementary reactions, whereas the C_2 mechanism considers both C_1 and C_2 species and involves 81 elementary reactions. The GRI-2.11 mechanism considers the chemistry of C_1 - and C_2 -species, involving 279 reactions and 49 species. The GRI-3.0 is the updated version of GRI-2.11 and involves 325 elementary reactions and 53 species. Differences between the two versions are outlined in on-line data at <http://www.me.berkeley.edu/gri-mech/>. The 12-step mechanism has been reduced from GRI-Mech 1.2 and validated by Sung et al.² for different combustion phenomena.

Results of our previous investigation¹ indicated that although all five mechanisms qualitatively reproduced the double-flame structure associated with PPFs there were significant quantitative differences between the flame structure obtained using the C_1 and C_2 mechanisms and that obtained using the GRI-2.11, GRI-3.0, and 12-step mechanisms. In particular, for low to moderate strain rates and high levels of air premixing ($\phi < 2.0$) the rich premixed reaction zone for the GRI-2.11, GRI-3.0, and 12-step mechanisms was located very close to the fuel nozzle and the physical separation between the two reaction zones was significantly larger compared to that for the C_1 and C_2 mechanisms. (Fuel nozzle here refers to the nozzle supplying the fuel-rich mixture. Also, the axial distance for presenting the computed and measured profiles in the present Note is measured from the fuel nozzle.) A lack of experimental data precluded making any definite conclusions as to which mechanism provided a more realistic prediction of the partially premixed flame structure. In the present investigation we employ experimental data of Osborne³ to further examine and validate these mechanisms. Because there were not significant differences between the predictions of C_1 and C_2 mechanisms and between the predictions of GRI-2.11, GRI-3.0, and 12-step mechanisms, we focus here on validating the C_2 and GRI-3.0 mechanisms.

Results and Discussion

The counterflow methane–air partially premixed flame was computed using the Oppdif⁴ and Chemkin⁵ packages. Details regarding these packages can be found elsewhere.^{1,4,5} An optically thin radiation model was incorporated into the original code to account for the radiation heat loss. Details are provided elsewhere.¹

Measurements

Nonintrusive laser diagnostics are used to study methane–air partially premixed flames in a counterflow burner.⁶ The burner is based on a previous design by Trees et al.⁷ A similar configuration has also been developed by Mastorakos et al.⁸ to examine the extinction behavior of turbulent counterflow flames. Measurements of species, including CH_4 , CO_2 , CO , O_2 , N_2 , and H_2O , and temperature are made axially from the exit of the methane–air jet, through the flame zone, to the exit of the airjet with spontaneous Raman scattering induced by a 20-ns laser shot from a narrowband tunable KrF excimer laser (200 mJ at 248 nm). The laser beam is focused by a 2-m lens to a 0.7×0.3 mm cross section in the measurement volume. Spontaneous Raman-scattered light from CH_4 , CO_2 , CO , O_2 , N_2 , and H_2O molecules is collected by $f/1.5$ Cassegrain optics and focused onto the entrance slit of a $\frac{1}{2}$ -m Spex spectrometer. The spectrometer entrance slit collects light from a 0.2-mm length of the laser beam. Thus, the measurement volume is $0.7 \times 0.3 \times 0.2$ mm. The spectrometer spectrally separates the light and focuses the diffracted images of the slit onto a Princeton Instruments intensified charge-coupled device.

Measurements of the opposed flow flame are made by applying the calibrated Raman system to the counterflow burner. Flames with equivalence ratio of 1.4 and strain rates of 100, 150, and 200 s^{-1} are measured. Data sets, each containing 310 shots, are recorded and averaged for consecutive positions along the axial dimension (stagnation streamline) of the burner. The spatial resolution along the stagnation streamline is 0.3 mm. The UV Raman setup, calibration

Received 21 June 2001; revision received 7 January 2002; accepted for publication 25 February 2002. Copyright © 2002 by the American Institute of Aeronautics and Astronautics, Inc. All rights reserved. Copies of this paper may be made for personal or internal use, on condition that the copier pay the \$10.00 per-copy fee to the Copyright Clearance Center, Inc., 222 Rosewood Drive, Danvers, MA 01923; include the code 0001-1452/02 \$10.00 in correspondence with the CCC.

*Graduate Assistant, Department of Mechanical Engineering, 842 W. Taylor Street.

†Professor, Department of Mechanical Engineering. Associate Fellow AIAA.

‡Engineer.

§Professor and Head, Department of Mechanical Engineering. Member AIAA.